Int. J. Solids Structures Vol. 30, No. 10, pp. 1355–1368, 1993
Printed in Great Britain

0020–7683/93 $6.00+ .00

BENDING STRESS ENHANCEMENT IN MATERIALS WITH LIMITED SHEAR RESISTANCE—PART I. SLIPPING-LAYERS MODEL

P. S. STEIF and A. TROJNACKI
Department of Mechanical Engineering, Carnegie Mellon University, Pittsburgh, PA 15213, U.S.A.

(*Received* 30 *December* 1991; *in revised form* 4 *November* 1992)

Abstract—Enhanced bending stresses in fiber composites that have a low longitudinal shear strength are studied theoretically. In Part I we investigate the response of a beam consisting of discrete layers which are coupled by friction. After presenting a general method of analysing such a beam, we give results for the specific case of three-point bending. The enhancement of the bending stresses is highlighted. Since the analysis of discretely layered beams is extremely time consuming, a much simplified theory is presented in Part II for an unlayered beam which is weak in longitudinal shear. The connection between the discretely layered beam and the shear-weak unlayered beam is demonstrated, and the simplified theory is used to infer the bending stress enhancement which is to be expected in practice.

1. INTRODUCTION

Continuous fiber ceramic-matrix composites are currently under active investigation as candidate materials for high-temperature structural applications. In contrast to traditional monolithic ceramics, these materials can be relatively insensitive to flaws; this is strongly dependent, however, on having the adequate interfacial properties, in particular relatively weak bonding at the fiber–matrix interface (Prewo *et al.*, 1986; Davidge, 1987; Hillig, 1987). Unfortunately, the improved flaw resistance is confined to loadings involving tension parallel to the fibers; the strength under off-axis tension and in longitudinal shearing is low when the fiber–matrix interface is weak. For example, in unidirectional carbon fiber-reinforced glasses, tensile strengths (parallel to the fibers) up to 1000 MPa can be achieved while shear strengths, measured in short beam shear tests, are only of the order of 20–35 MPa (Prewo, 1988). Under off-axis loadings, the matrix bears the brunt of the load, and the weak interface serves as a source of flaws. While the transverse tensile strength can be improved through lamination, the longitudinal shear properties are likely to persist.

Low longitudinal shear strength has a number of negative implications for composite response. We consider here one consequence which could have significant practical implications, particularly since longitudinal shearing generally accompanies bending. To motivate our study, imagine the transverse loading of a deck of n playing cards, each having thickness $h = H/n$ (see Fig. 1). If the cards stick to one another, then the deck deflects like a solid beam of thickness H [see Fig. 1(a)]. Assuming the cards are elastic, the maximum stress would be $3PL/2bH^2$. However, if the cards slip freely with respect to one another, then each card deflects like a beam of thickness H/n under a maximum bending moment $PL/4n$ leading to a maximum stress of $3nPL/2bH^2$ [see Fig. 1(b)]. Consequently, the maximum sustainable load P is potentially much less (n times less) in the freely slipping case than in the sticking case. This simple demonstration suggests the potential significance of a more detailed investigation into the tendency for shear slippage to augment bending stresses in weakly bonded fiber composites. While this effect is related to the well-appreciated weak longitudinal shear properties, it appears not to have been recognized previously in the literature. Of course, a weakly bonded fiber composite under bending differs from the deck of cards in that stresses arise which resist longitudinal shearing.

The present two-part paper is an attempt to quantify the bending stress enhancement which occurs in materials that have limited shear resistance. Two distinct approaches to modeling the weakness in shear are adopted. In Part I we consider a model which views the

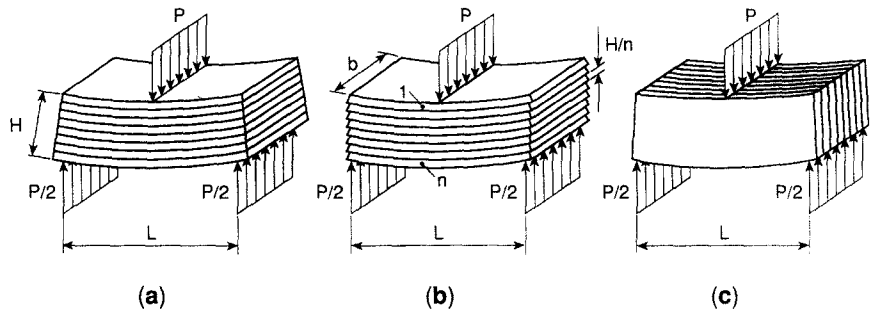

Fig. 1. Transverse loading of a layered solid. (a) Unslipping (bonded) layers; (b) Slipping layers; (c) Edge-on loading.

weakly bonded unidirectional fiber composite as a set of discrete layers which have a finite inter-layer shear strength τ_p. Once this shear strength is reached, relative slip can occur at the interface, while the shear stress remains at τ_p, as would be the case for a frictional interface.

In fact, the composite is reasonably viewed as a set of layers, at least when fabricated by the standard technique of stacking infiltrated fiber tows and hot-pressing. Furthermore, these inter-layer surfaces are likely to be the planes which are weakest in shear. This is evident from short beam shear tests on carbon-reinforced glasses (Prewo, 1988), which reveal lower longitudinal shear strengths when the composite is deformed in the normal fashion than when the loading is "edge-on" [see Fig. 1(c)]. Our assumption that the interlayer shear stress remains at some value (τ_p) during sliding is based on the notion that the shear stress is partially frictional in origin. To see the basis for this idea, note that the longitudinal shear strength of approximaely 25 MPa appears not to be wholly determined by the matrix strength, which is often substantially higher at, say, 100 MPa. Instead, the relatively weak frictional resistance of the fiber–matrix interface (typically of the order of 2–15 MPa) seems to play an important role in setting the longitudinal shear strength.

Although we present the equations governing the deformations of beams composed of discrete, frictionally coupled layers under general loadings, detailed calculations are carried out only for a specific loading equivalent to the three-point bend test. Nevertheless, this loading reveals a number of the interesting features peculiar to this class of materials. However, even with all the idealizations associated with beam-like deformations in each of the layers, obtaining solutions to the resulting equations for even the simplest loadings turns out to be extremely computationally intensive. This difficulty in obtaining solutions motivates Part II, in which we consider a second model, this time of a homogeneous (unlayered) beam with limited internal shear resistance. The second model results in far simpler equations to solve; interestingly, the results of the second model are shown to be equivalent to the results for the layered beam when the number of layers becomes large.

Relevant to the layered beams studied here in Part I are several contributions in the literature aimed at analyzing laminated structures with imperfect bonding. A number of authors have considered adhesively bonded layered beams, in which the relative tangential displacement of two neighboring layers is proportional to the shear stress in the thin connecting adhesive film (Goodman and Popov, 1968; Fazio *et al.*, 1982; Murakami, 1984). An extreme case of this was considered by Rao and Ghosh (1980) in which adjacent layers are completely unconnected except at the ends. Sheinman and Soffer (1991) applied an earlier derived theory (Sheinman and Adan, 1987) to investigate the effect of a delamination of constant length on the imperfection sensitivity of laminated beams. Some aspects of the stability of two-layer beam-columns with interfacial frictional slippage were considered by Krzys and Trojnacki (1989). The same authors (Krzys and Trojnacki, 1990) also considered the influence of slip on the buckling of a layered ring with initial imperfections, with particular regard to damping in the structure. In none of these papers has the effect of shear slippage on the bending stresses been examined.

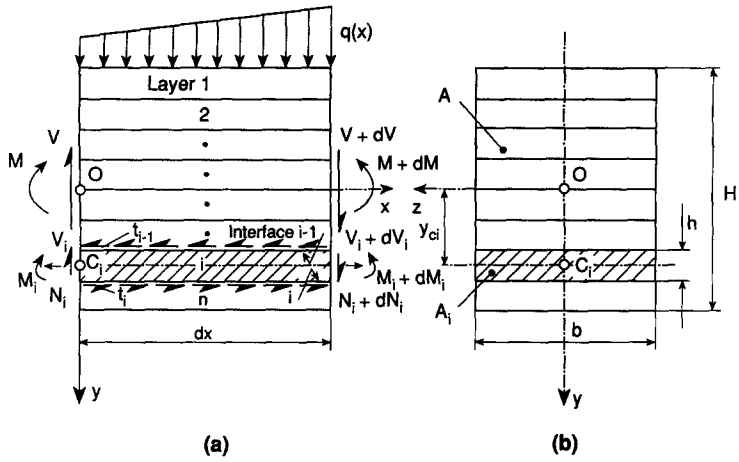

Fig. 2. (a) Definition of overall stress resultants, layer stress resultants, and interfacial shear stresses. (b) Definition of cross-sectional dimensions and layer centroid.

2. ANALYSIS

The typical geometry under consideration is shown in Fig. 2. A supported beam, consisting of n discrete layers of equal thickness h, is under a general loading of transverse forces and applied moments. For convenience, the layers are numbered $i = 1, 2, \ldots, n$ from top to bottom, while the interfaces are numbered $i = 1, 2, \ldots, n-1$ from top to bottom. The layers are elastic and orthotropic (with respect to the layer boundaries). The displacements are continuous from one layer to the next, provided the shear stress is less than the interfacial strength τ_p. Once this shear strength is reached, tangential displacement discontinuities are possible and the shear stress remains at τ_p; normal displacements are assumed to remain continuous (no separation of layers). The analysis is carried out under the obvious generalization of the Bernoulli hypothesis for beams: we assume that "plane sections remain plane" for each of the layers individually. Shear deformations are neglected, and the standard engineering theory for shear stresses in beams of rectangular cross-section is used. As a consequence, the longitudinal stress σ must vary linearly with y in each layer, and the shear stress τ varies parabolically with y in each layer. Nothing precludes the layers from having different moduli and thicknesses, or τ_p from varying from one interface to another or with respect to x; in what follows, however, we do not treat this more general case. Of interest are the stresses in the layers, and the deflection of the beam.

At some cross-section x, let the loading of the beam give rise to net bending moment M and net shear force V; the net axial force N is assumed to be zero. (Note that within the general formulation, it is possible that the stress resultants are not immediately derivable from the loads, i.e. the problem may be statically indeterminate in the usual sense.) Furthermore, let the individual layer resultants N_i, M_i and V_i be defined in terms of the normal stress $\sigma(y)$ and shear stress $\tau(y)$ distributions as follows:

$$N_i = \iint_{A_i} \sigma(y)\, \mathrm{d}A, \tag{1a}$$

$$M_i = \iint_{A_i} \sigma(y)(y - y_{ci})\, \mathrm{d}A, \tag{1b}$$

$$V_i = \iint_{A_i} \tau(y)\, \mathrm{d}A, \tag{1c}$$

for $i = 1, 2, \ldots, n$, where y_{ci} denotes the y-coordinate of the centroid (center) of the cross-sectional area $A_i = bh$ of the ith layer. The individual layer resultants are connected with the overall resultants by

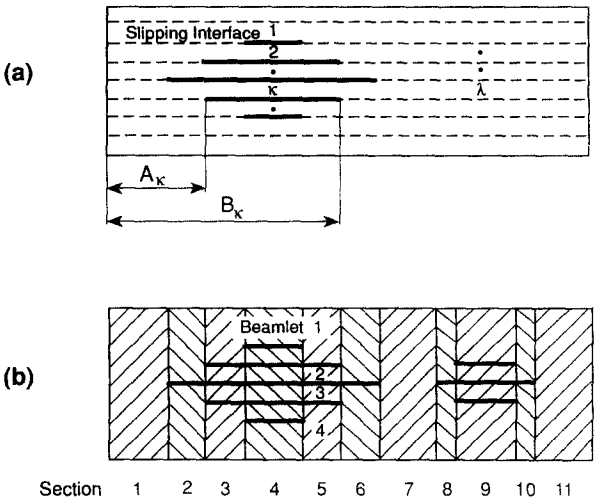

Fig. 3. (a) Definition of slip zones. (b) Definition of beamlets and sections.

$$\sum_{i=1}^{n} N_i = 0, \tag{2a}$$

$$\sum_{i=1}^{n} (M_i + N_i y_{ci}) = M, \tag{2b}$$

$$\sum_{i=1}^{n} V_i = V. \tag{2c}$$

Crucial to a solution of the problem of a frictionally coupled layered beam is identifying the portions of the different interfaces which have reached shear stress τ_p and are slipping. These portions of the interfaces are called slip zones. A determination of slip zones is complicated by the fact that problems featuring frictional slip depend on the history of loading. For simplicity, we envision a monotonically increasing loading, with all distributed as well as concentrated loads increasing with a single scalar parameter. When the solution is obtained for a gradually increasing load, it is possible to track each of the slip zones as it appears. Therefore, one can assume that at any instant the number of slip zones (if any) along each interface is known. To be determined are the exact locations of the ends of all slip zones. The left and right end points are denoted by A_κ and B_κ ($\kappa = 1, 2, \ldots, \lambda$), respectively, where λ is the total number of slip zones. A schematic of the layers and the slip zones is shown in Fig. 3(a). As seen below, the entire stress distribution also emerges from the correct calculation of A_κ and B_κ.

The iterative procedure by which the end points are found starts with some initial (guessed) values for A_κ and B_κ. The procedure then views the beam as divided into sections ($\nu = 1, 2, \ldots, \eta$) as shown in Fig. 3(b), in which $\eta = 11$. Each section consists of a set of 1 or more "beamlets". These beamlets have horizontal bounding surfaces which are free surfaces of the entire beam and/or slipping interfaces. The layer interfaces within each beamlet are not slipping. For example, in a section with no slipping interfaces [1, 7 and 11 of Fig. 3(b)], the beamlet is the entire beam cross-section; in sections with a single slipping interface [2, 6, 8 and 10 of Fig. 3(b)], there are two beamlets which meet at the slipping interface, and so forth.

First, it should be noted that the stresses can be immediately derived for sections having no slip zones. Such sections deform as a single solid beam, with a linear distribution of normal stress that is statically equivalent to the local bending moment $M(x)$. To see this, recall that by assumption each layer deforms like a beam with a linear variation in the normal stress (corresponding to a layer axial force N_i and a layer bending moment M_i). Since there is no slip between the interfaces, the axial strain at the interfaces must be continuous. Also, continuity of deflections between adjacent layers means that the curvature

is the same. Together, these kinematic conditions at all interfaces imply that the distribution of strain (and stress) across the layers is a single and continuous linear function in y.

Consider now a section possessing $m-1$ slipping surfaces and, thus, m beamlets. We will follow the convention that a subscript i ($i = 1,2,\ldots,n-1$) denotes a generic interface (or layer), while a subscript j ($j = 1,2,\ldots,m-1$) will denote a generic slipping interface (or beamlet). In no case will the summation convention on repeated indices be used; any summation will be indicated explicitly. Let t_j ($j = 0,1,\ldots,m$) denote the shear stresses bounding the beamlets; specifically the jth beamlet is bound by t_{j-1} and t_j. These shear stresses are known: for the free surfaces of the whole beam $t_0 = t_m = 0$, and for the internal surfaces which are, by definition, slipping,

$$|t_j| = \tau_p, \quad (j = 1,2,\ldots,m-1). \tag{3}$$

With the beamlet resultants N_j and M_j ($j = 1,2,\ldots,m$) defined by equations analogous to (1), conditions of equilibrium for each beamlet are

$$\frac{dN_j}{dx} = (t_{j-1} - t_j)b, \tag{4a}$$

$$\frac{dM_j}{dx} = V_j - \tfrac{1}{2}(t_{j-1} + t_j)bh_j, \tag{4b}$$

for $j = 1,2,\ldots,m$, where h_j is the thickness of the jth beamlet.

Since there is complete displacement continuity across the non-slipping interfaces which constitute the interior of each beamlet, according to an argument given above each beamlet deforms as a solid beam. Alternatively, since every non-slipping interface is within a beamlet, having each beamlet deform as a solid beam guarantees displacement continuity at all non-slipping interfaces. In fact, we enforce such a deformation in all beamlets.

To determine the stresses in the beamlets within a single section, consider now the no-separation condition across the slipping interfaces which divide each beamlet from its neighbor. This condition implies that the vertical deflections w_j (from the initial position) of all beamlets in a cross-section x must be identical. (In fact, the vertical deflection w_i of every layer must be the same in a cross-section x; as mentioned above, this will be automatically enforced within each beamlet.) This condition can be written as

$$w_j(x) = w_{j^*}(x), \quad (j = 1,2,\ldots,m), \tag{5}$$

where j^* is any single fixed integer from among $1,2,\ldots,m$. Higher order derivatives of w_j with respect to x are also continuous across all interfaces, in particular the second and third derivatives.

Now, since the beamlets deform as solid beams, one can relate the second derivative of w_j (the curvature) to the bending moment by the usual elastic relation:

$$EI_j \frac{d^2 w_j}{dx^2} = -M_j, \quad (j = 1,2,\ldots,j^*,\ldots,m), \tag{6}$$

where I_j is the second moment of inertia of the jth beamlet, and E is the modulus of elasticity (assumed constant).

Combining the constitutive law (6) and the equilibrium equation (4b), one then obtains

$$\frac{d^3 w_j}{dx^3} = -\frac{1}{EI_j}(V_j - T_j), \quad (j = 1,2,\ldots,j^*,\ldots,m), \tag{7}$$

where $T_j = (t_{j-1} + t_j)bh_j/2$. The third derivative of the conditions of continuity of displacements (5) with d^3w_j/dx^3 replaced by (7) constitutes now a set of $m-1$ independent

relations for the beamlet shear forces V_j. A trivial equality holds when $j = j^*$. If these relations are rearranged into the form

$$V_j = \frac{I_j}{I_{j^*}}(V_{j^*} - T_{j^*}) + T_j, \quad (j = 1, 2, \ldots, j^*, \ldots, m), \tag{8}$$

then summation over the index j for $j = 1, 2, \ldots, m$ (holding j^* fixed) and use of eqn (2c) as appropriate to beamlets, yields the following expression for V_j:

$$V_j = \frac{I_j}{\sum_{j=1}^{m} I_j}\left(V - \sum_{j=1}^{m} T_j\right) + T_j, \quad (j = 1, 2, \ldots, m). \tag{9}$$

From V_j and the bounding shear stresses t_j, one can compute the shear stress $\tau_j(y)$ in the jth beamlet, remembering that each beamlet deforms as a solid beam and, therefore, has a parabolic distribution:

$$\tau_j(y) = a_0 + a_1 y + a_2 y^2, \tag{10}$$

where $j = 1, 2, \ldots, m$, and

$$a_0 = t_{j-1} - a_1\left(y_{cj} - \frac{h_j}{2}\right) - a_2\left(y_{cj} - \frac{h_j}{2}\right)^2,$$

$$a_1 = -\frac{(t_{j-1} - t_j)}{h_j} - 2a_2 y_{cj},$$

$$a_2 = -6\frac{(V_j - T_j)}{bh_j^3}.$$

The procedure outlined thus far must be applied to every section, with the result that all relevant conditions are satisfied *within* each section. From the shear stresses, the axial force and the bending moment in each beamlet can be computed with the use of eqns (4) to within two constants, $C_j^{(v)}$ and $D_j^{(v)}$, respectively:

$$N_j^{(v)} = (t_{j-1}^{(v)} - t_j^{(v)})bx + C_j^{(v)}, \tag{11a}$$

$$M_j^{(v)} = \int V_j^{(v)}\,dx - T_j^{(v)}x + D_j^{(v)}, \tag{11b}$$

for $v = 1, 2, \ldots, \eta$; $j = 1, 2, \ldots, m$. The superscript (v) refers to a generic section, and the subscript j refers to a beamlet within that section. It should be noted that the total number of beamlets m within any specific section changes from one section to the next.

For each section, these constants are constrained by two equations: the net axial force is zero, and the net moment is $M(x)$. It remains to enforce the appropriate kinematic and static conditions *between* sections; that is, the deformed beamlets in adjacent sections must fit together, and the normal stress must be continuous across sections. It is these continuity conditions which constrain the extents of the slipped zones.

We first state the conditions that must be satisfied and then justify the conditions. Let $\Delta\varepsilon_\kappa(x)$ represent the strain across the κth slipping interface. Then, for $\kappa = 1, 2, \ldots, \lambda$, the following equations must hold:

$$\int_{A_\kappa}^{B_\kappa} \frac{\partial \Delta\varepsilon_\kappa}{\partial x}\,dx = 0, \tag{12a}$$

$$\int_{A_\kappa}^{B_\kappa} \Delta\varepsilon_\kappa\,dx = 0. \tag{12b}$$

To see the basis for eqns (12), consider re-assembling the beam, section by section, while attempting to maintain continuity of displacement and traction. As discussed above, the normal stress distribution (a single linear function of y) is determined in the solid section 1 from the local bending moment $M(x)$. The two constants which set the axial force and bending moment in each of the two beamlets in section 2 are determined by continuity of axial force and bending moment across each of the two halves of the section 1–section 2 interface. (Note, first, that with a linear stress profile in each beamlet, continuity of axial force and bending moment ensures complete continuity of normal stress. Secondly, continuity of all the stress resultants ensures that the two equations for the net axial force and the net moment are automatically satisfied in section 2.) Continuity of displacement is trivial; one only needs to place the beamlets in section 2 flush against those in section 1. This fixes the rigid body displacement and rotation which have to be applied in section 2 beamlets in the reassembling process.

The identical procedure is carried out for subsequent sections up to and including the section with the maximum number of beamlets [4 in Fig. 3(b)]. Now, consider the beamlets in the next section (5). Can the beamlets in this section be attached to the previous section which had a greater number of beamlets? This question is obviously critical in the case of the top beamlet and bottom beamlet: each of these beamlets must be consistent with the stresses and displacements associated with *two distinct* beamlets in section 4. In other words, the deformations in, say, the top two beamlets of section 4, must be such that *together* they give rise to a *single* linear distribution in stress at their right end (against section 5). As explained below, this requirement is fulfilled when eqn (12a) is satisfied. Furthermore, the right faces of these two beamlets must form a single planar surface, to enable the beamlet in section 5 to be placed flush. This requirement is fulfilled when eqn (12b) is satisfied.

Consider first the connection between eqn (12a) and the distribution of stress. In order to have a single linear distribution in the normal stress at the right side of the upper *two* beamlets in section 4, we need to have continuity of strain and continuity of the strain derivative (with respect to y) across their slipping interface at the right side. Continuity of the strain derivative would come from continuity of curvature. In fact, the beamlet shear forces in a given section were derived by forcing the continuity of d^3w_j/dx^3—the derivative of the curvature with respect to x—across the slipping interface between the beamlets. Since the curvature at the left side of the beamlets was made continuous (when we assembled the beamlets in section 4), the curvature at the right side (and all along the slipping interface) will automatically be continuous. With regards to continuity of strains, these are, in general, discontinuous across the slipping interface. They were forced, however, to be continuous at the left side of the beamlet when we asssembled section 4. By satisfying eqn (12a), we force the strain to be once again continuous across the slipping interface at the right side of the beamlets, i.e. at the section 4–section 5 interface.

We turn now to displacement continuity. The right side of the upper two beamlets in section 4 must constitute a single planar surface. This means that the displacement u_x and the derivative of u_x with respect to y must be continuous across the slipping interface at the right side. Recall that in assembling the beamlets in section 4, we were required to give them a common slope at their left face, because they were placed flush against a common single beamlet. Of course, we were free to do this. Then, continuity of curvature across the entire slipping interface (which we established above), immediately implies a common slope at the right faces of the beamlets. Likewise, we were required (and permitted) to give the upper two beamlets in section 4 the same displacement at the slipping interface at the left side. While the displacement is not continuous at most points across the slipping interface, eqn (12b) forces the displacement to be once again continuous at the right side of the upper two section 4 beamlets.

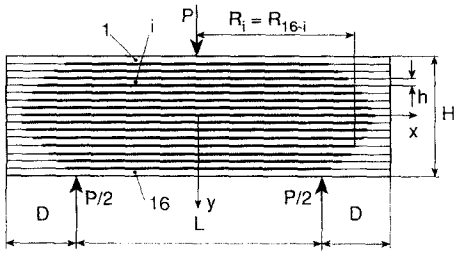

Fig. 4. Definition of beam dimensions and slip zones for three-point bending.

The set of equations given thus far is complete. Given the current values for the extents of the slip zones, one computes $V_j^{(v)}$ from eqn (9), which leads to the shear stresses [eqn (10)]. One then computes $N_j^{(v)}$ and $M_j^{(v)}$ from eqns (11), to within the constants $C_j^{(v)}$ and $D_j^{(v)}$. The normal stress is then found from

$$\sigma_j(x,y) = \frac{M_j(x)}{I_j}(y-y_{cj}) + \frac{N_j(x)}{A_j}, \quad (j = 1,2,\ldots,m), \tag{13}$$

which yields, in turn, the strain $\varepsilon_j = \sigma_j/E$. One then attempts to satisfy all conditions of normal stress continuity between sections, in addition to eqns (12). If they cannot be satisfied, then the extents of the slip zones need to be altered and the process repeated.

Unfortunately, we have been unable to discover a solution method appropriate to, say, a general distributed transverse load $q(x)$. The primary difficulty lies in the necessity of describing the locus of slip surfaces. For a general $q(x)$ there can be multiple slip zones along each interface. To proceed further, therefore, we have chosen to investigate a rather specific loading, in particular three-point bending with a monotonically increasing load (see Fig. 4). For this particular loading, the set of equations that must be satisfied is given in the Appendix. Note that the beam depicted in Fig. 4 extends a distance D beyond the supports. While such a portion would simply displace and rotate rigidly in standard beam theory, it plays a more significant role here. First, we find that there are stresses in this portion of the beam, though the net stress resultants are zero. Second, the presence of this portion actually alters the stresses in the central part of the beam. This is dealt with in more detail below.

3. RESULTS AND DISCUSSION

In discussing the results we will focus on the particular geometry of $L/H = 5$, $D/L = 0.267$ and $n = 16$. While the effect of the overhang D/L will be explained below, a discussion of the dependence on the number of layers n and on the aspect ratio L/H is postponed until Part II. Since the number of layers is 16, there are 15 interfaces, with one interface (number 8) coinciding with the center of the beam. There are distinct levels of load P which are of interest: P_{si} which denotes the load at which slip initiates at the ith interface, and P_{ci} at which slip along the ith interface extends to $|x| = L/2+D$. From the solution for a solid beam, one can determine P_{s8} to be $4bH\tau_p/3$; at this load, slip is initiated simultaneously along the entire interval $|x| < L/2$ of the central (eighth) interface. Values for other P_{si} and P_{ci} are arrived at through the solution of the equations given in the Appendix. The slip zone boundaries r_1 to r_8 (where $r_i = R_i/L$ and R_i, the half-length of the slip extent on the ith interface, are defined in the Appendix) are shown in Fig. 5 as functions of dimensionless load $p = P/P_{s8}$ (by symmetry, $r_{16-i} = r_i$ for $i = 1,2,\ldots,7$). It is interesting to compare, for example, the load to initiate slip on the top interface $P_{s1}/P_{s8} = 1.531$ with the prediction based on the shear stresses in a solid beam, which gives 4.267. The difference gives the effect of neglecting the presence of all the other slip surfaces.

We consider next the distributions of normal (bending) stress in the beam. To do this it is useful to separate the loading into four stages. In stage I, slip has occurred on some, but not all, interfaces, and none of the slip regions extends to $|x| = L/2+D$. In stage II,

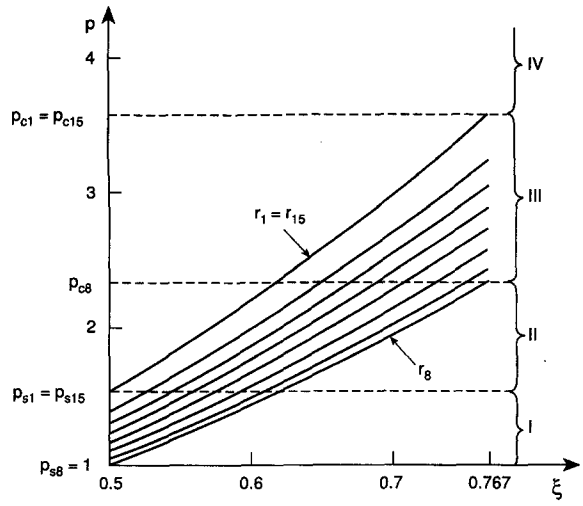

Fig. 5. Extent of slip on each interface for various levels of dimensionless load $p \equiv P/P_{s8}$ for three-point bending; stages I, II, III, IV are shown.

slip has occurred on all interfaces, but has not reached $|x| = L/2+D$ on any interface. In stage III, the slip region extends to $|x| = L/2+D$ on at least one, but not all, interfaces. In stage IV, slip on all interfaces extends to $|x| = L/2+D$. (Stage IV is akin to the deck of cards except there is inter-card friction.) Note that for smaller values of D/L the sequence of events can be different, namely complete slip on the inner interfaces can occur prior to slip initiation on the outer interfaces.

For each of the four stages, we have plotted (in Fig. 6) the normal stress distribution in each layer on the "tensile" side of the beam ($y > 0$) at $x = 0$; the stress is normalized by the maximum stress in a solid beam under the same load. For low loads (stage I), there is slip in the central portion of the beam. One should note that there are compressive stresses (admittedly small) in the central layers, while the stresses are still wholly tensile in the four outer layers (which are acting as a solid beam). The stress in the outermost fiber is slightly greater (at approximately 30%) than the maximum stress in a solid beam under the same load. By stage II, some slip has occurred on every interface, and even the outermost layer exhibits some compressive stress (on its inner side). The maximum stress is nearly four times that in a similarly loaded solid beam. Note that even in the central layers, the maximum tension (and compression) exceeds the solid beam's maximum stress by over a factor of two.

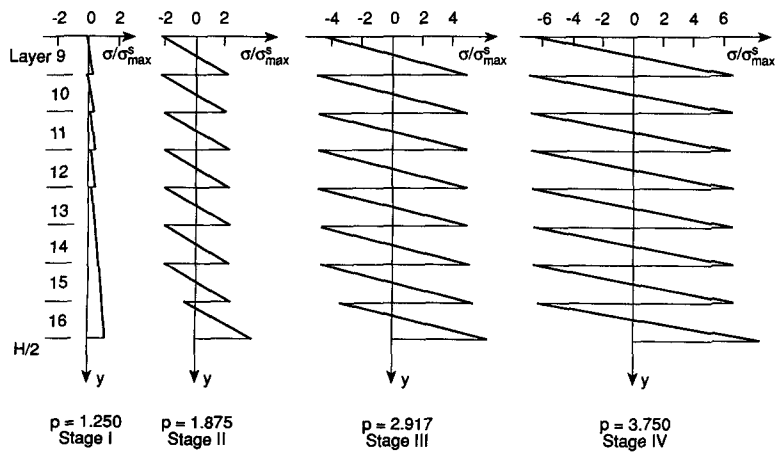

Fig. 6. Axial stress in lower half of beam at central cross-section ($x = 0$) for four stages of loading.

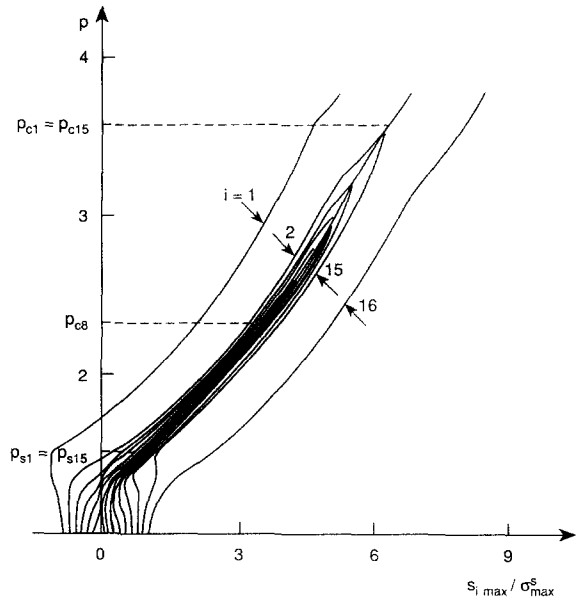

Fig. 7. Maximum axial stress in each layer at central cross-section ($x = 0$) for various levels of dimensionless load p.

Once some of the slip zones reach the ends of the beam (stage III), the stresses in these layers are identical, with the maximum being substantially higher than the solid beam's maximum. Extra enhancement of the tensile stress occurs in the outermost layer. By stage IV, all layers have identical stress distributions, except for the outer one which has a greater tensile stress and a lesser compressive stress. This can be seen in a different way in Fig. 7, where the stress $s_{i\max}$ ($i = 1, 2, \ldots, 16$) on the positive side of each layer (point in layer where y is maximum) is plotted as a function of the normalized load p.

We consider now the effect of an overhang—a portion of the beam ($|x| > L/2$) beyond the supports. As indicated above, there are stresses in the overhang. These are shown in Fig. 8, where the normal force and bending moment in layer 12, for example, are plotted as functions of $\xi = x/L$, along with the deflection of the entire beam. For comparison, the force and moment distributions from the solid beam are shown as well. Clearly, the layer carries a force and moment even in the overhang. Also, the deflection is not a rigid body rotation in the overhang, but involves curvature. The stress distribution through the entire cross-section is shown in Fig. 9 for the overhang ($\xi = 0.527$) and at the center ($\xi = 0$).

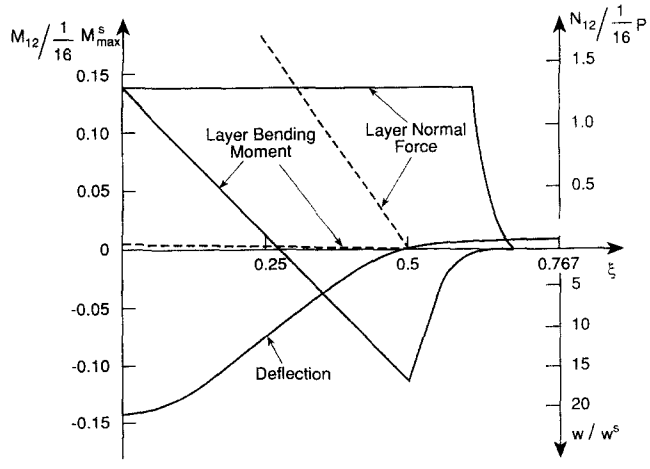

Fig. 8. Axial variation in layer bending moment and normal force (12th layer) and beam deflection ($p = 1.875$ and $M^s_{max} = PL/4$; ——— discretely layered beam, – – – solid beam).

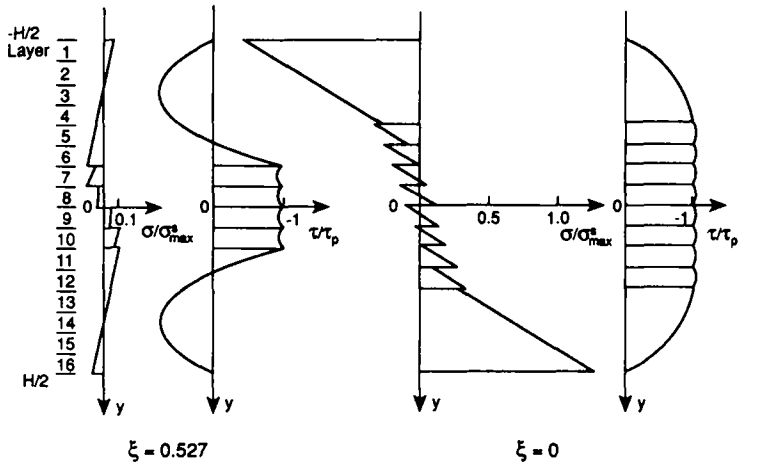

Fig. 9. Distribution of axial and shear stresses in overhang (where net stress resultants are zero) and at center cross-section ($p = 1.25$).

Figure 10 indicates the effect of the size of the overhang $d = D/L$ on the mid-point deflection; the influence on the stress distribution at the mid-point can be seen in Fig. 11. (The calculation of the deflection requires an additional parameter τ_p/E; the value $\tau_p/E = 30$ MPa/130 GPa $= 2.308 \times 10^{-4}$ was used.) It is clear that the overhang serves to increase the beam's resistance to transverse loadings which produce shear slippage. This can be understood by considering the simple case of a two-layer beam in which the slip zone has propagated to the ends of the beam. Of interest is the difference between a large and small overhang. The presence of the interfacial shear stress τ_p causes there to be an axial tension in the lower layer and compression in the upper layer. The magnitude of this axial force increases linearly with the total length $L/2+D$. This tension and compression contribute to the bending moment; the larger the axial forces, the less must be the bending moment in each layer, since the total maximum bending moment is fixed at $PL/4$. Since the layer bending moment gives rise to the deflection and to the bulk of the stress, extending the overhang effectively stiffens and strengthens the beam against bending.

4. CONCLUSIONS

Fiber-reinforced composites are often rather weak in longitudinal shearing. This can magnify the *axial* stresses when the composite is subjected to loads which cause bending.

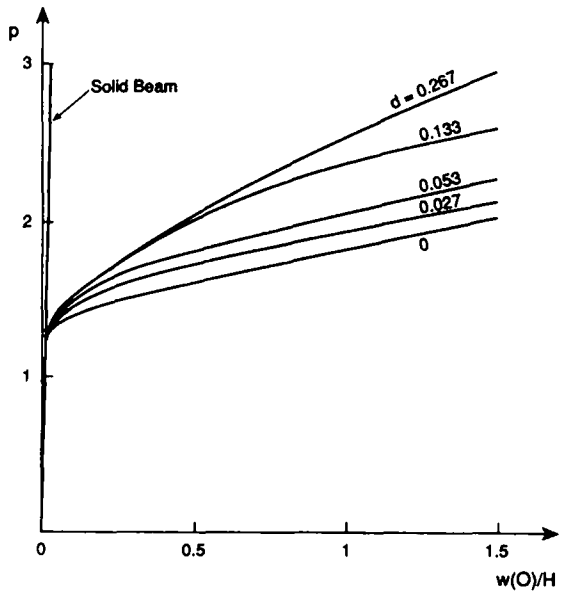

Fig. 10. Load–deflection curves for various extents of overhang ($\tau_p/E = 2.308 \times 10^{-4}$).

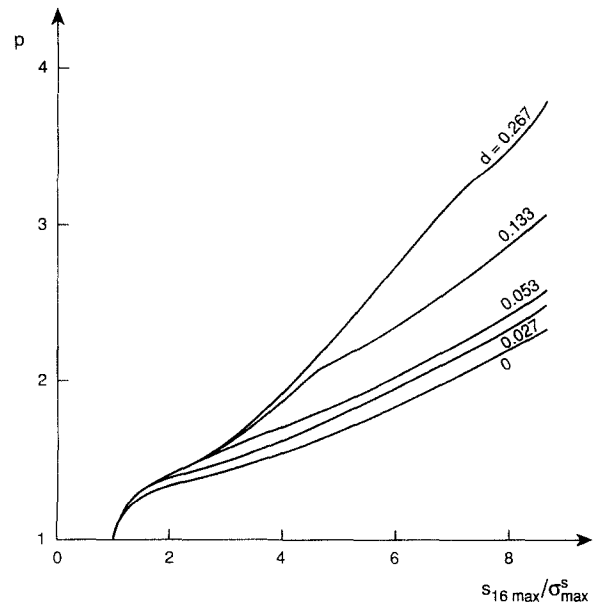

Fig. 11. Maximum axial stress in slipping beam at central cross-section ($x = 0$) normalized by maximum axial stress in solid beam for various degrees of overhang.

In order to understand this effect, we have studied the model problem of a beam composed of layers that are coupled by friction. We have presented a method of analysing such beams subjected to the standard loadings; each layer is treated with the simplest of beam theories and no inter-layer separation is permitted. Crucial to calculating the stress distribution is a determination of the locations of the slip zones on each interface.

The general method of analysis was applied to the particular case of a beam under three-point bending. Once the applied load reaches levels at which inter-layer slip begins, the stress distribution and the deflection begin to differ from those of a solid beam under the same loading. The differences become substantial as the load increases; eventually the stresses, both tensile and compressive, become enormously magnified in all layers. Interestingly, the presence of a portion of the beam extending beyond the supports (an overhang) has the effect of stiffening and strengthening the beam—an effect completely absent in standard beam theory. While the very substantial stress enhancements that occur when slip has extended to the edge of the specimen might be of concern, it is also possible that the composite being represented would already be considered to have failed in shear. This drawback of the layered beam model, as well as the fact that it is time consuming to analyze, motivate the simplified theory which is presented in Part II.

Acknowledgements—We appreciate the assistance provided by Mr R. Landers in carrying out the computations. P.S.S. was supported by Air Force Office of Scientific Research grant 890548 and A.T. was supported by Department of Energy grant DE-FG02-89ER45404. Assistance provided by General Electric Aircraft Engines and by the Department of Mechanical Engineering, Carnegie Mellon University is also gratefully acknowledged.

REFERENCES

Davidge, R. W. (1987). Fibre-reinforced ceramics. *Composites* **18,** 92–98.

Fazio, P., Hussein, R. and Ha, K. H. (1982). Sandwich beam-columns with inerlayer slips. *Proc. ASCE, J. Engin. Mech. Div.* **108,** No. EM2, 354–366.

Goodman, J. R. and Popov, E. P. (1968). Layered beam systems with interlayer slip. *Proc. ASCE, J. Struct. Div.* **94,** No. ST11, 2535–2547.

Hillig, W. B. (1987). Strength and toughness of ceramic matrix composites. *Ann. Rev. Mater. Sci.* **17,** 341–383.

Krzys, W. and Trojnacki, A. (1989). Stability of layered column allowing for slips along interlayer surfaces of contact. *Arch. Mech. Engng* **36,** 217–238.

Krzys, W. and Trojnacki, A. (1990). Stability of layered ring with layers bonded by friction. *Arch. Mech. Engng* **37,** 5–21.

Murakami, H. (1984). A laminated beam theory with interlayer slip. *ASME J. Appl. Mech.* **51,** 551–559.

Press, W. H., Flannery, B. P., Teukolsky, S. A. and Vetterling, W. T. (1990). *Numerical Recipes in C*. Cambridge University Press, Cambridge, New York.

Prewo, K. M. (1988). Carbon fibre reinforced glass matrix composite tension and flexure properties. *J. Mater. Sci.* **23**, 2745–2752.

Prewo, K. M., Brennan, J. J. and Layden, G. K. (1986). Fiber reinforced glasses and glass-ceramics for high performance applications. *Am. Cer. Soc. Bull.* **65**, 305–314.

Rao, K. M. and Ghosh, B. G. (1980). Imperfectly bonded unsymmetric laminated beam. *Proc. ASCE, J. Engng Mech. Div.* **106**, No. EM4, 685–697.

Sheinman, I. and Adan, M. (1987). The effect of shear deformation on post-buckling behaviour of laminated beams. *ASME J. Appl. Mech.* **54**, 558–462.

Sheinman, I. and Soffer, M. (1991). Post-buckling analysis of composite delaminated beams. *Int. J. Solids Structures* **27**, 639–646.

APPENDIX

In this Appendix we present the set of equations pertaining to a simply-supported layered beam with a concentrated force applied in the center (three-point bending). Under this loading, the three concentrated forces result in discontinuities in the shear force $V(x)$. It is convenient, therefore, to extend the definition of a section introduced earlier. The terminal points of the slip zones (not known in advance) still demarcate the x locations of the boundaries between distinct sections; in addition, a concentrated external load (whose location is known) also demarcates the boundary between distinct sections. With this generalized definition of a section, each of the layer stresses is described by a single formula in each section.

In analysing the three-point bend test one can take advantage of symmetries, as well as the fact that at most a single slip zone appears on each interface. Identical layer thicknesses and τ_p being constant imply symmetry about the center line; after the first slip appears at the central interface (number $n/2$), the next slips occur symmetrically about this interface. Furthermore, the extent of the slip zones is the same at interfaces located symmetrically about $y = 0$; the slip zones decrease in extent as one moves from the central interface towards the free surfaces of the beam. Taking advantage of the symmetry about $x = 0$, one finds that there are $\eta/2$ sections in $x > 0$, the first section being from $x = 0$ to the right support at $x = L/2$.

Some useful relationships simplifying the analysis can now be derived. When a load P results in $m^{(1)}$ beamlets in the section $0 < x < L/2$, the number of sections η is related to $m^{(1)}$ by $\eta = m^{(1)}+4$. Since there is a single slip zone at each interface, the total number of slip zones λ can be expressed in terms of $m^{(1)}$ as $\lambda = m^{(1)}-1$. Symmetry about $x = 0$ and eqn (12a) yields the relation $R_\kappa \equiv B_\kappa = -A_\kappa$ ($\kappa = 1, 2, \ldots, m^{(1)}-1$). Symmetry about $y = 0$ implies that the index κ can be replaced by i and expressed in terms of $m^{(1)}$ and the total number of layers n. With this substitution, the number of slipping segments of different extent, i.e. the number of unknown coordinates R_i [$i = (n-m^{(1)})/2+1, \ldots, n/2$] is also a function of $m^{(1)}$, namely it equals $m^{(1)}/2$. In all, the number of unknown extents of the slip zones is reduced by a factor of four. The number of beamlets in the vth section, $m^{(v)}$, can be viewed as a function of $m^{(1)}$, namely $m^{(v)} = m^{(1)}+2(2-v)$, ($v = 2, 3, \ldots, \eta/2$). The first (and last) beamlet in each section is composed of $(n-m^{(v)})/2+1$ unslipping layers, whereas the remaining $m^{(v)}-2$ beamlets consist of a single layer between two slipping interfaces. The first slip occurs at the interface $i = (n-m^{(v)})/2+1$, and the last one at the interface $i = (n+m^{(v)})/2-1$.

While the general method of analysis presented above is explained most clearly by introducing beamlets, the numerical procedure is more convenient when the equations refer to individual layers. The appropriate equations in each beamlet consisting of more than one layer are simply decomposed into sets of equations valid for each of the beamlet's layers. While this introduces more unknowns, the associated additional equations are obvious, since, as mentioned in the analysis section, beamlets deform like a single solid beam with complete continuity of strain and strain derivative. Admittedly, such a procedure enlarges the number of equations to be solved (except when all interfaces are slipping). It has the advantage, however, of giving a fixed number of equations (for given n), which means that complicated renumbering schemes, which would be necessary when the number of slipping interfaces change, are avoided.

The set of equations that must be satisfied reduces to $n\eta/2+m^{(1)}/2$ equations and is given by:

(i) $n\eta/2-n$ conditions expressing continuity of layer axial forces and layer bending moments across each of the boundaries between sections:

$$C_i^{(v)} = N_i^{(v+1)}(R_j)-(t_{i-1}^{(v)}-t_i^{(v)})bR_j, \tag{A1a}$$

$$D_i^{(v)} = M_i^{(v+1)}(R_j)-\int_0^{R_j} V_i^{(v)}\,dx+T_i^{(v)}R_j, \tag{A1b}$$

for $i = 1, 2, \ldots, n/2$; $v = 1, 2, \ldots, \eta/2-1$; $j = j(v) = \begin{cases} 0 & \text{for } v = 1, \\ (n-m^{(1)}/2-1+v & \text{for } v > 1; \end{cases}$

(ii) n conditions expressing vanishing layer axial forces and layer bending moments at the edge of the specimen (at $x = L/2+D$):

$$C_i^{(\eta/2)} = 0, \tag{A2a}$$

$$D_i^{(\eta/2)} = 0, \tag{A2b}$$

for $i = 1, 2, \ldots, n/2$;

(iii) $m^{(1)}/2$ conditions (12b) (the relative displacement must again be zero at the right end of the slip zones):

$$\int_0^{R_i}\left[\frac{6}{h}(M_i^{(v)}+M_{i+1}^{(v)})+N_i^{(v)}-N_{i+1}^{(v)}\right]\mathrm{d}x=0, \tag{A3}$$

for $i=(n-m^{(1)}/2+1,\ldots,n/2$; $v=1,2,\ldots,\eta/2$, where $R_0=L/2$ and $N_i^{(v)}$ and $M_i^{(v)}$ must be calculated separately in each section. (Note that the lower limit of integration in (A3) is zero; this is a consequence of the symmetry, which makes the relative displacement zero at $x=0$.)

We now give expressions for layer shear forces $V_i^{(v)}$ and interfacial shears $t_i^{(v)}$. (From these quantities, one can determine the axial forces and bending moments, and then axial stresses and axial strains.) For multi-layer beamlets, the shear forces are given by

$$V_i^{(v)}=b\int_{-\{n-2(i-1)\}h/2}^{-(n-2i)h/2}(\alpha_0+\alpha_1 y+\alpha_2 y^2)\,\mathrm{d}y, \tag{A4}$$

for $i=1,2,\ldots,(n-m^{(v)})/2+1$; $v=1,2,\ldots,\eta/2$, where

$$\alpha_0=\tfrac{1}{2}nh(\alpha_1-\tfrac{1}{2}nh\alpha_2),$$

$$\alpha_1=\tfrac{1}{2}h\alpha_2(n+m^{(v)}-2)+\frac{2\tau_p}{(n-m^{(v)}+2)h},$$

$$\alpha_2=-\frac{12}{bh^3}\frac{2V_1^{(v)}-(n+m^{(v)}-2)bh\tau_p}{(n-m^{(v)}+2)^3+4(m^{(v)}-2)},$$

$$V_1^{(v)}=\tfrac{1}{6}bh\tau_p(n-m^{(v)}+2)\frac{2n(n-m^{(v)}+2)^2p-3(m^{(v)}-2)[(n-m^{(v)}+2)^2-2]}{(n-m^{(v)}+2)^3+4(m^{(v)}-2)},$$

and for single-layer beamlets these shear forces are given by

$$V_i^{(v)}=\tfrac{1}{3}bh\tau_p\frac{8np+3(n-m^{(v)}+2)[(n-m^{(v)}+2)^2-2]}{(n-m^{(v)}+2)^3+4(m^{(v)}-2)}, \tag{A5}$$

for $i=(n-m^{(v)}/2+2,\ldots,n/2$; $v=1,2,\ldots,\eta/2$, where $p=3P/4bH\tau_p$ is the non-dimensional loading and in sections $v>1$ we have $p=0$.

Interfacial shears are given by

$$t_i^{(v)}=\begin{cases}0 & \text{for } i=0,\\ \alpha_0+\alpha_1 y_i^{(v)}+\alpha_2(y_i^{(v)})^2 & \text{for } i=1,2,\ldots,\dfrac{n-m^{(v)}}{2},\\ \tau_p & \text{for } i=\dfrac{n-m^{(v)}}{2}+1,\ldots,n/2,\end{cases} \tag{A6}$$

for $v=1,2,\ldots,\eta/2$, where $y_i^{(v)}=-(n-2i)h/2$.

A numerical solution consists of two parts: given the load P, one must determine the total number of slip zones (directly related to $m^{(1)}$, the number of beamlets in the first section), and the extents of the slip zones R_i $[i=(n-m^{(1)})/2+1,\ldots,n/2]$. The numerical technique takes advantage of the monotonic nature of the loading, which means that the total number of slip zones increases monotonically with the loading. Say that the number of slip zones is known at the current level of the load. Then, one must solve the $m^{(1)}/2$ equations (A3), which are non-linear in the unknowns R_i, subject to eqns (A1) and eqns (A2), which are $n\eta/2$ linear constraints on the integration constants $C_j^{(v)}$ and $D_j^{(v)}$. This set of equations was solved using Powell's (Press *et al.*, 1990) optimization procedure. At each increment in the load P, the distribution of shear stresses in the midspan region $|x|<L/2$ must be checked. If the shear stress has reached (or exceeded) τ_p on the next interface, then $m^{(1)}$ is incremented.